BRAIN
ORIGINAL ARTICLE

The bidirectional lung brain-axis of amyloid-β pathology: ozone dysregulates the peri-plaque microenvironment

Hendrik J. Greve,[1] August L. Dunbar,[1] Carla Garza Lombo,[1] Chandrama Ahmed,[1] Morrent Thang,[1] Evan J. Messenger,[1] Christen L. Mumaw,[1] James A. Johnson Jr,[1] Urmila P. Kodavanti,[2] Adrian L. Oblak[3] and Michelle L. Block[1,4]

The mechanisms underlying how urban air pollution affects Alzheimer's disease (AD) are largely unknown. Ozone (O_3) is a reactive gas component of air pollution linked to increased AD risk, but is confined to the respiratory tract after inhalation, implicating the peripheral immune response to air pollution in AD neuropathology. Here, we demonstrate that O_3 exposure impaired the ability of microglia, the brain's parenchymal immune cells, to associate with and form a protective barrier around Aβ plaques, leading to augmented dystrophic neurites and increased Aβ plaque load. Spatial proteomic profiling analysis of peri-plaque proteins revealed a microenvironment-specific signature of dysregulated disease-associated microglia protein expression and increased pathogenic molecule levels with O_3 exposure. Unexpectedly, 5xFAD mice exhibited an augmented pulmonary cell and humoral immune response to O_3, supporting that ongoing neuropathology may regulate the peripheral O_3 response. Circulating HMGB1 was one factor upregulated in only 5xFAD mice, and peripheral HMGB1 was separately shown to regulate brain *Trem2* mRNA expression. These findings demonstrate a bidirectional lung-brain axis regulating the central and peripheral AD immune response and highlight this interaction as a potential novel therapeutic target in AD.

1 Department of Pharmacology and Toxicology, The Stark Neurosciences Research Institute, Indiana University School of Medicine, Indianapolis, IN, USA
2 Cardiopulmonary and Immunotoxicology Branch, Public Health and Integrated Toxicology Division, U.S. Environmental Protection Agency, Research Triangle Park, NC, USA
3 Department of Radiology and Imaging Sciences, The Stark Neurosciences Research Institute, Indiana University School of Medicine, Indianapolis, IN, USA
4 Roudebush Veterans Affairs Medical Center, Indianapolis, IN, USA

Correspondence to: Michelle L. Block, PhD
Department of Pharmacology and Toxicology, Stark Neurosciences Research Institute
Indiana University School of Medicine
320 West 15th Street, NB 214D, Indianapolis
IN 46202, USA
E-mail: mlblock@iupui.edu

Keywords: air pollution; amyloid plaque; microglia; TREM2; lung-brain axis; HMGB1

Introduction

Rapidly increasing in global prevalence,[1] Alzheimer's disease (AD) is the leading form of dementia and disease-modifying treatments are unavailable,[2] emphasizing the urgent need to understand AD aetiology and pathophysiology. Increasing reports indicate environmental influence in AD aetiology, where multiple components of urban air pollution associated with cardiovascular and pulmonary disease are now linked to an increased risk of AD,[3–5] but the underlying biological mechanisms and how they may affect AD neuropathology are poorly understood.

Received August 23, 2021. Revised February 07, 2022. Accepted February 27, 2022. Advance access publication March 28, 2022
Published by Oxford University Press on behalf of the Guarantors of Brain 2022.

Amyloid-beta (Aβ) levels accumulate and condense into plaques within the brain parenchyma,[6] where Aβ plaques are a hallmark of AD and one driver of disease-associated damage. Recent work points to an association between ambient air pollution exposure and an increased Aβ PET signal in humans,[7] but there is significant debate regarding how urban air pollution could affect Aβ pathology, the extent of the effect, and the neuropathological consequences. Prior work in animal models focuses on detrimental Aβ processing,[8–10] but the effect on Aβ clearance is unknown.

Microglia, the innate immune cells of the brain parenchyma, have been previously implicated as key mediators of the CNS effects of air pollution exposure due to their production of pro-inflammatory factors,[11–14] a process also typified in AD neuropathogenesis.[15] In addition, as a critical response to Aβ pathology in AD, a subset of microglia known as disease-associated microglia (DAM) migrate to, associate with, and form barriers around amyloid plaques to restrict plaque growth and clear Aβ, due largely to triggering receptor expressed on myeloid cells 2 (TREM2).[16–19] At present, the impact of air pollution on microglial plaque association is undefined.

Urban air pollution is comprised of several components, including the reactive gas ozone (O_3), which is incapable of translocating to the brain,[20,21] but has been associated with an increased AD risk and cognitive decline.[4,22,23] Previous work points to a lung-brain axis in this process, where the pulmonary response to O_3 exposure indirectly regulates the CNS neuroimmune function in part through circulating and cellular factors.[24,25] The impact of O_3 and the lung-brain axis on Aβ plaque pathology has yet to be tested. Importantly, a handful of human studies support a link between AD and pulmonary comorbidities, such as chronic obstructive pulmonary disease (COPD) and asthma,[26] but how the lung-brain axis and the response to air pollution change during AD processes is unexplored.

Currently, the mechanisms of how O_3 signals to the CNS and the effects on AD pathology remain largely unknown. Using 5xFAD mice, we sought to address how a subchronic O_3 exposure affects AD pathology, neuroinflammation, neurotoxicity, the peri-plaque microenvironment and the lung-brain axis. Further, we identify a previously unknown bidirectional aspect of the lung-brain axis and HMGB1 as a likely significant circulating factor for communicating along the lung-brain axis.

Materials and methods

Reagents

Rabbit anti-ionized calcium-binding adaptor molecule 1 (IBA-1, 1:500) antibody was procured from Wako Chemical (Cat. No. 019-19741, RRID: AB_839504). Sheep anti-mouse TREM2 (1:300; Cat. No. AF1729, RRID: AB_354956) antibody was obtained from R&D systems. Mouse anti-human β-amyloid (clone 6e10; Cat. No. 803001, RRID: AB_2564653), HRP conjugated mouse anti-human $Aβ_{1-40}$ (Cat. No. 805407, RRID: AB_2564979), and HRP conjugated mouse anti-human $Aβ_{1-42}$ (Cat. No. 805507, RRID: AB_2564980) antibodies were purchased from BioLegend. Rat anti-mouse lysosomal-associated membrane protein 1 (LAMP1; Clone 1D4B) antibody was purchased from Abcam (Cat. No. ab25245, RRID: AB_449893). All other reagents were procured from Sigma-Aldrich.

Mice

Male transgenic 5xFAD mice and littermate controls (WT) on a C57Bl/6J background were obtained from the Jackson Laboratory (Stock: 034848). The 5XFAD transgenic mice robustly develop amyloid pathology,[27] as they overexpress five familial Alzheimer's disease (FAD) mutations: the APP (695) transgene contains the Swedish (K670N, M671L), Florida (I716V), and London (V717I) mutations; the PSEN1 transgene contains the M146L and L286V FAD mutations. Because female 5xFAD mice exhibit a markedly higher amyloid pathology that increases over time,[28,29] which is believed to be partially artificial and confounded due to the oestrogen response element in the *Thy1* promoter, which drives the transgene expression in 5xFAD mice,[27,29–31] only male mice were assessed. The C57Bl/6J (Stock: 000664) and *LysM*-Cre (Stock: 004781) mice were purchased from Jackson Laboratory. HMGB1 floxed mice[32] were obtained from Riken (BRC No. RBRC06240). To generate $Hmgb1^{fl/fl}$*LysM*-cre^{+} mice, $Hmgb1^{fl/fl}$ mice were mated with *LysM*-$Cre^{+/+}$ mice, and $Hmgb1^{fl/fl}$*LysM*-Cre^{-} littermates were used as controls. All $Hmgb1^{fl/fl}$*LysM*-Cre mice were genotyped to confirm presence or absence of cre recombinase. Mice were individually housed in micro-isolator cages in an AAALAC-accredited housing facility maintained on a 12 h light/dark cycle at 20–24°C. Mice were acclimated to the housing facility for at least 1 week prior to the beginning of studies. Experimental mice were individually housed in HEPA-filtered, ventilated polycarbonate cages and food and water were provided to the mice *ad libitum*. A total of 60 5xFAD and 60 WT mice were used in this study. For the first experiment, 30 5xFAD and 30 WT were assigned to treatment groups in a randomized block design, with 10 mice per group to assess traditional amyloid pathology and serum profiles. In a separate experiment, an additional 30 5xFAD and 30 WT mice were assigned to treatment groups in a randomized block design, with 10 mice per group to assess bronchoalveolar lavage immune profiles and for the PFA fixed brains for digital spatial profiling analysis. To determine the role of HMGB1 in *Trem2* expression, 35 $Hmgb1^{fl/fl}$*LysM*-cre^{+} and 35 $Hmgb1^{fl/fl}$*LysM*-cre^{-} mice were assigned as 17–18 mice per treatment group. Finally, to assess the impact of recombinant HMGB1, 14 C57Bl/6J mice were assigned to treatment groups in a randomized block design, with seven mice per group. All experiments were approved by the IACUC (IUSM 11325 and 11327) and were in accordance with the NIH guidelines for housing, breeding, and experimental use. All mice were treated humanely with regard for alleviation of suffering.

Ozone exposure

O_3 was generated via an HFL-10 O_3 generator (Ozonology) and mice were exposed in a whole body, Rochester Hinners style, stainless steel and glass, 0.3 m^3 whole body chambers. The O_3 concentration was continuously monitored using a UV photometric O_3 analyzer (465L, Teledyne API) and temperature was maintained at 21 ± 2°C. Rodents are insensitive to O_3 toxicity,[33,34] owing to their complex nasal turbinates,[33,35] lung morphological differences, and high urate and ascorbate concentrations in the airway surfactant. For these reasons, a factor of 3 is accepted practice for extrapolating concentrations between primates and rodents.[34] O_3 concentrations of 0.2–0.3 ppm are frequently achieved in areas of high air pollution, where 1 ppm is considered the equivalent in rodent experiments O_3.[24]

To determine the effects of O_3 exposure on AD neuropathology, we employed a subchronic model of O_3 exposure previously used.[36,37] Two experiments were performed ($n = 10$ mice per group) for two separate end points: lung and brain. Male 10–11-week-old 5xFAD and littermate control mice were habituated to O_3 exposure chambers for 5 days prior to the start of the experiment by exposing all mice to filtered air only. Mice were placed in wire-mesh cages and exposed to O_3 (0.3 ppm or 1.0 ppm) or filtered air control for 4 h/day,

three consecutive days/week for 13 weeks in Rochester-style Hinners Chambers. For short term O_3 exposures, male 6–8-week-old *Hmgb1*$^{fl/fl}$*LysM*-cre mice ($n = 36$ *Hmgb1*$^{fl/fl}$*LysM*-cre^{-}, 33 *Hmgb1*$^{fl/fl}$ *LysM*-cre^{+}) were habituated to chambers for 5 days and exposed for 4 h/day, three consecutive days. At 24 h after final exposure, animals were euthanized with isoflurane for sample collection.

rHMGB1 administration

Male C57Bl/6J aged 6–8 weeks ($n = 8$ per group) received a single injection by tail vein of rHMGB1 (32.5 μg in 200 μl, Thermo Scientific; Cat. No. 34-8401-85) or vehicle (20 mM Tris-HCL, pH 8.0, 0.2 M NaCl, 1 mM DTT) control. Three hours after injection, brains were collected and dissected for analysis by RT-qPCR.

Brain tissue collection

Twenty-four hours after the final O_3 exposure or 3 h after rHMGB1 injection, mice were anaesthetized with isoflurane by open-drop method,[38,39] and blood and brains were collected. The right hemisphere of each brain was drop-fixed in 4% paraformaldehyde for 2 days followed by cryopreservation in 30% sucrose. The left hemisphere was microdissected into separate brain regions, snap frozen in liquid nitrogen, and stored at –80°C until analysis.

Collection and analysis of bronchoalveolar lavage fluid

Mice were euthanized 24 h after the final exposure by isoflurane overdose by open-drop method and bronchoalveolar lavage fluid (BALF) was collected from mice by lavaging the lung twice with 1 ml of Hank's balanced salt solution (HBSS) without Ca^{2+} or Mg^{2+}. After collection, BALF was centrifuged at $1500 \times g$ for 10 min at 4°C, and the supernatant from the first lavage was collected for biochemical analysis while the cells from both lavages were pooled together for cellular analyses by resuspending in 250 μl of phosphate-buffered saline (PBS). Total cell counts were determined using a TC-10 automated cell counter (Bio-Rad), and cells were centrifuged onto slides using a Shandon Cytospin centrifuge (Thermo Scientific). Cells were differentially stained using Wright-Giemsa and cell differentials were determined by a blinded observer counting at least 400 cells at 40× per sample. The remaining cells from the bronchoalveolar lavage were snap frozen and stored at –80°C until NanoString RNA analysis.

Immunohistochemistry

Cryopreserved right hemispheres were sectioned on a freezing stage microtome at 40 μm. For Thioflavin S (ThioS) staining and Aβ (6e10, 1:500) plaque load analyses, every 12th section through a hemibrain was stained. ThioS staining was performed by immersing slide-mounted sections in 1% filtered ThioS in 50% EtOH for 10 min at room temperature, followed by two washes in 80% EtOH for 3 min each, followed by one wash in 95% EtOH for 3 min, followed by three washes in diH20 for 3 min each. For 6e10 staining, sections first underwent antigen retrieval by incubating in sodium citrate for 15 min at 85°C, followed by 30 min at room temperature to cool. Sections were then washed 3× in PBST followed by blocking in 5% normal goat serum for 1 h at room temperature. Sections were then incubated in primary antibody solution overnight at 4°C. Sections were then washed 3× in PBST followed by incubation in secondary Alexa-Fluor antibodies (1:1000) for 1 h at room temperature protected from light. Sections were then washed 3× in PBST, placed on slides and mounted with ProLong™ Gold. LAMP1 and IBA-1 staining was performed on four evenly spaced brain sections as described above. For TREM2 immunohistochemistry, four evenly spaced sections per brain underwent antigen retrieval using Reveal Decloaker (Biocare Medical) for 15 min at 85°C followed by room temperature for 30 min. Sections were then blocked in 5% normal donkey serum containing mouse on mouse blocking solution (MOM, 1:1000) for 1 h at room temperature. Sections were then incubated with primary antibodies for 2 days at 4°C. Sections were then washed 3× in PBST followed by incubation with secondary antibodies for 6 h at room temperature protected from light. Sections were washed 3× in PBST and sections were placed on slides. Slides were mounted with ProLong™ Gold. To determine ThioS and 6e10 plaque load, whole slides were scanned using a Leica Aperio Versa slide scanner at 10× objective. Images were analysed in ImageJ where regions of interest (ROIs) were drawn around the whole cortex and hippocampus. Images were manually thresholded and the analyse objects function was used to quantify per cent areas and plaques per area in each region. Z-stacks of LAMP-1/ThioS were acquired at 20×, spaced 1 μm apart, on a Nikon A1R confocal microscope in the M1/M2 regions of the cortex. Images were analysed using Nikon Advanced Research NIS analysis software to determine the per cent area of LAMP-1 positivity of maximum intensity projections. Z-stacks of TREM2/IBA-1/6e10 were acquired at 40× on a Nikon A1R confocal microscope in the M1/M2 regions of the cortex. Each optical section was spaced 1 μm apart. Z-stacks were collapsed into a single image using NIS elements software and individual ROIs were drawn around each plaque. The amount of TREM2 on IBA-1+ microglia was calculated around each plaque and normalized to the plaque area. The number of plaque-associated microglia were counted manually around each plaque per frame. The total number of microglia per image were manually counted. For analysis of microglia morphology in rHMGB1 experiments, Z-stacks spaced 1 μm were collected in the somatosensory cortex and midbrain of 4 IBA-1 stained sections at 40×. Analysis was performed as previously described to obtain the average microglial volume.[40] All image analysis was performed by blinded analysts.

Brain sample processing for ELISA and RT-qPCR

Brain regions (whole cortex, hippocampus, midbrain) were first extracted in tissue protein extraction reagent (T-PER, Thermo Fisher Scientific) supplemented with protease and phosphatase inhibitors (Roche Diagnostics). For RNA analyses, an equal amount of homogenate was mixed with TRIzol™ reagent and extraction was performed according to manufacturer's instructions. Aβ extraction was performed as previously described.[41] An equal amount of homogenate was mixed with 0.4% diethylamine (DEA) and underwent high speed centrifugation at $135\,000 \times g$ for 1 h at 4°C. Supernatant was mixed with 0.5 M Tris-HCl (10:1, sample to Tris-HCL), and snap frozen on dry ice for analysis of soluble fraction. The remaining pellet was solubilized in cold formic acid with sonication, and then centrifuged at $105\,000 \times g$ for 1 h at 4°C. Supernatant was neutralized in formic acid neutralization buffer (1 M Tris-base, 0.5 M Na_2HPO_4) and snap frozen on dry ice for analysis of the insoluble fraction.

Microglia isolation

Microglia were isolated as previously described.[40] Briefly, mice were anaesthetized with a ketamine/xylazine cocktail and transcardially

perfused with cold PBS. Brains were dissociated using the Neural Tissue Dissociation Kit (P) (Miltenyi Biotec; Cat. No. 130-092-628), and microglia were isolated by magnetic column separation using CD11b microbeads (Miltenyi Biotec; Cat. No 130-049-601) to select for microglia.

Intraperitoneal macrophage isolation

For preparation of peritoneal macrophages, mice were injected with thioglycollate solution (3.8%, IP). Three days post-injection, the peritoneal cavity was lavaged with MACS buffer (PBS, 1% BSA, 1 mM EDTA) and the cells were collected for RNA, as previously reported.[42]

ELISA

For Aβ ELISAs, MaxiSorp ELISA plates were coated overnight with 6e10 antibody at 4°C. Plates were washed (PBS, 0.025% Tween20) 4× and blocked in 1% skim milk for 1 h at 37°C. Plates were washed 4× and samples or standards were loaded in duplicate and plates were incubated overnight at 4°C with shaking. Plates were washed 4× and incubated with HRP-conjugated detection antibodies for 1 h at room temperature. Plates were washed 4× and developed with TMB colorimetric solution and stopped with 2 N H_2SO_4. Plates were read at 450 nm. For HMGB1 ELISAs, protocol was followed according to manufacturer's protocol. NfL ELISA (MesoScale Discovery, Cat No. F217X-3) was run according to manufacturer's instructions.

RT-qPCR

TRIzol™ extracted RNA was treated with DNaseI using Ambion DNA-free kit (Thermo Scientific-Invitrogen). RNA was reverse transcribed using Maxima First Strand cDNA Synthesis Kit (Thermo Fisher Scientific). PowerUp Sybr Green Master Mix (Life Technologies) or TaqMan Advanced Fast Master Mix (Life Technologies) were used. For Sybr Green probes, 500 nM forward and reverse primers were used. Sequences for primers were *Gapdh* forward 5′-GAACATCATCCCTGCATCCA-3′ and reverse 5′-CCAGTGAGCTTCCCGTTCA-3′, *Il1b* forward 5′-TGAAGAAGAGC CCATCCTCTGTGA-3′ and reverse 5′-GGTCCGACAGCACGAGGC TT-3′, *Trem2* forward 5′-TGGGACCTCTCCACCAGTT-3′ and reverse 5′-GTGGTGTTGAGGGCTTGG-3′, and *Nlrp3* forward 5′-ATTACCCGC CCGAGAAAGG-3′ and reverse 5′-TCGCAGCAAAGATCCACACAG-3′. TaqMan probes were used according to manufacturer's instructions. TaqMan probes were used for *Slc18a3* (Mm00491465_s1), *Chat* (Mm00491465_s1), *Ache* (Mm00477275_m1), and *Gapdh* (Mm99999915_g1). *Gapdh* was used as the housekeeping gene for all RT-qPCR experiments, and data were calculated using the $2^{-\Delta\Delta CT}$ method. Quantitative PCR was performed on a Viia7 (Life Technologies) RT-PCR system.

Milliplex array

To examine serum cytokine/chemokine changes, a MilliPlex Mouse Cytokine/Chemokine 32-Plex panel was used (Millipore-Sigma). Serum samples were thawed and centrifuged at $10\,000 \times g$ for 10 min and then run according manufacturer's instructions. Samples were analysed on a Bio-Plex 200 System (Bio-Rad Laboratories).

NanoString nCounter gene expression panels

For analysis of mRNA in BAL cells, NanoString Mouse Immunology Panels were used (NanoString Technologies). RNA was extracted from BAL cells using RNeasy Micro kits (Qiagen), and 75 ng/sample were hybridized to probes according to manufacturer's instructions. NanoString Panels were run using nCounter Max/Flex system. Data were analysed in nSolver Advanced Analysis Software.

NanoString digital spatial profiling

Paraformaldehyde fixed 10 µM sections were incubated with the NanoString proprietary cocktail comprised of two tissue markers (amyloid beta and microglia) and approximately 60 antibodies (Neural Cell Profiling Core, Alzheimer's Disease Panel, Alzheimer's Disease Extended Panel, Glial Subtyping Panel) with unique photo-cleavable oligonucleotide tags. Using NanoString's GeoMx™ Digital Spatial Profiler system,[43] Aβ plaques and microglia were identified using fluorescently labelled antibodies against Aβ and IBA-1. Amyloid plaques in the M1/M2 region of the cortex were selected and a 100 µm diameter circular ROI was placed around the plaque core, the amyloid positive plaque was then segmented out of the ROI to only leave the immediately adjacent area for collection within the 100 µm diameter ROI, defining the peri-plaque microenvironment. As an internal control tissue, a 100 µm diameter ROI was placed in the cortex with microglial staining and no plaque. Using the GeoMx DSP, these selected areas were individually UV illuminated to photocleave the oligonucleotides within each ROI. The resulting oligonucleotides were collected in a 96-well plate by the GeoMX DSP. After collection the wells were then hybridized according to the manufacturer's instructions and analysed on the nCounter® platform, resulting in distinct spatially mapped counts that correspond to the antibodies from which the tags were cleaved. Count data first underwent quality control for system variation and then normalized to control protein counts. Protein changes were assessed as a change from the peri-plaque ROI compared to the non-plaque ROI. Radial heatmaps were generated using Complex Heatmaps package in R as previously described.[44]

Statistical analysis

Sample size for experiments were determined based on prior reports and power analyses. A randomized block design was employed for all animal experiments, and sample processing was performed blind, where the code denoting groups was only provided for data analysis. Data were analysed in GraphPad Prism 8.0 (GraphPad Prism, San Diego, CA, USA). Data are expressed as the mean ± standard error of the mean (SEM). Outliers were determined to be points that were outside of the mean ± 2 standard deviation (SD) and were removed from all subsequent analyses, except for GeoMX data, which were determined using the ROUT method with Q = 1%. Gaussian distribution of data was evaluated by using D'Agostino-Pearson normality testing, where $P > 0.05$ indicated a normal distribution. Mean differences were analysed by Bonferroni's *post hoc* analysis, or Welch's *t*-test, when appropriate. A P-value < 0.05 was considered statistically significant. For Nanostring RNA data, Benjamini-Hochberg FDR corrections were used for the generation of volcano plots. For Nanostring GeoMX data, to account for multiple ROIs for each mouse, a linear mixed model was used to evaluate protein expression using the GeoMX DSP data analysis package. For each analysis, the protein expression levels were used as the dependent variable with a single fixed effect [O_3 versus filtered air (FA), peri-plaque versus non-plaque], and mouse ID was used as the random effect with random intercept. A P-value < 0.05 was considered statistically significant.

Data availability

The data in this manuscript are available upon reasonable request to the corresponding author.

Results

Ozone exposure impairs microglial-plaque association

Microglia cells surround and clear plaques through a transcriptomic shift regulated by TREM2,[18,45] where studies indicate that the loss of this phenotype exacerbates amyloid pathology.[19,46] To begin to explore whether air pollution (O_3) affects the ability of microglia to interact with plaques, 5xFAD mice were exposed to O_3 (0.3 or 1.0 ppm) or FA control for 13 weeks. Examination of the plaque microenvironment by confocal microscopy showed decreases in plaque-associated microglia without changes in the total number of microglia (Fig. 1A–C). Further, the amount of TREM2 protein localized around amyloid plaques was decreased (Fig. 1D). However, normalizing the TREM2 expression to IBA-1 expression shows no change in TREM2 levels (Fig. 1E), supporting that decreased TREM2 may be due to reduced microglia in the peri-plaque environment, rather than microglial loss of TREM2. Representative images taken in the hippocampus further supports that O_3 impairs microglial-plaque association in multiple brain regions (Supplementary Fig. 1).

Examination of pro-inflammatory marker expression by qPCR in the cortex showed increases in the pro-inflammatory genes *Nlrp3* and *Il1b* (Fig. 1F), two components of the inflammasome that are upregulated in AD.[47,48] While O_3 showed no changes in cortical *Trem2* mRNA expression (Fig. 1F), this failure to change may note pathology. More specifically, while increasing ThioS staining in the cortex is significantly correlated with increasing levels of *Trem2* mRNA expression in filtered air-exposed 5xFAD mice, this association is abolished with O_3 (1 ppm) exposure (Fig. 1G), suggesting amyloid plaque-driven increases in TREM2 expression may be perturbed with O_3 exposure. As such, these are the first data to demonstrate that O_3 exposure impedes microglial plaque association, impairs plaque-associated increases in gene expression of the master DAM regulator TREM2, and may impede the plaque-restricting DAM phenotype.

Ozone exposure exacerbates amyloid pathology

In an effort to determine the pathological significance of O_3-impaired microglia-plaque association, we next examined the effects of O_3 exposure on amyloid pathology. We observed an increase in the number of dense-core ThioS+ plaques (Fig. 2A and B) and the number of diffuse 6e10+ plaques (Fig. 2C and D) in both the cortex and hippocampus. Further consistent with the loss of plaque restricting microglia, we also observed an increase in the size of diffuse 6e10+ plaques in the cortex and hippocampus (Fig. 2E). Cortical mRNA expression of human *APP* (hAPP) was unchanged by O_3 exposure (Supplementary Fig. 2A), and examination of Aβ isoforms showed only increases in insoluble $Aβ_{42}$ only in the hippocampus (Supplementary Fig. 2B). However, there was a significant shift in the ratio of $Aβ_{42}$ to $Aβ_{40}$in the cortex (Fig. 2F), suggesting aberrant changes to Aβ processing after O_3 exposure. Taken together, these data demonstrate that an environmentally relevant, subchronic O_3 exposure exacerbates plaque number, size, and load, in addition to shifting the $Aβ_{42}/Aβ_{40}$ratio, supporting an effect of air pollution on microglial plaque restriction, Aβ processing, and potentially microglial clearance.

Ozone exposure augments amyloid-induced neuron damage

We next aimed to understand if the increase in amyloid pathology and decreased microglial-plaque association after O_3 exposure exacerbated amyloid-associated neuronal toxicity. To investigate the effects of O_3 on neuronal pathology, we stained for LAMP-1 as a marker of dystrophic neurites,[49] and ThioS for dense-core plaque (Fig. 3A). We observed an increase in the amount of plaque-associated LAMP-1 (Fig. 3B), demonstrating an increase of dystrophic neurites. To further explore the consequences of O_3 exposure, we investigated components of the acetylcholinergic pathway. In order to explore the effects of O_3 on the acetylcholinergic system, we examined mRNA expression of three key components in the cortex: choline acetyltransferase (ChAT), vesicular acetylcholine transporter (Slc18a3), and acetylcholinesterase (AChE) (Fig. 3C). We observed decreases in the expression of all three components in only 5xFAD mice, suggesting that O_3 exposure perturbs a key neurophysiological pathway relevant to AD. Examination of serum levels of neurofilament light (NfL), a marker of neurodegeneration,[50] did not show significant increases in response to O_3 exposure in 5xFAD mice (Supplementary Fig. 3). Together, these findings support that the O_3 exposure augments neuropathology that is linked to amyloid deposits.

Ozone exposure alters the peri-plaque microenvironment and dysregulates the DAM phenotype

Using digital spatial profiling to image and spatially resolve proteomic changes (Fig. 4A), we next sought to identify how the O_3-associated neuropathology was altered by plaque localization in the cortex. When comparing protein changes in peri-plaque versus non-plaque areas, in addition to a core protein signature shared by both exposures (green), there was a unique signature of protein changes noted in the cortical peri-plaque region of mice exposed to FA (blue) and O_3 (red) (Fig. 4B). Radial heat maps of peri-plaque (inner circle) and non-plaque (outer circle) of FA and O_3 proteins detail these unique proteomic signatures in O_3-exposed cortices (Fig. 4C). Volcano plots reveal that O_3 dysregulates the dynamic protein differences documented between non-plaque and peri-plaque regions (Fig. 4D). To focus on microglial protein expression, including DAM markers, protein expression was normalized to CSF1R, a homeostatic marker shown not to change with DAM stage,[18] for microglial proteins. The Venn diagrams (Supplementary Fig. 4A and B) further detail that when compared to non-plaque regions, the peri-plaque region in 5xFAD mice exhibits a dynamic microglial protein response to plaques that includes DAM protein markers; a responsivity that is partially lost with O_3exposure. These O_3 changes support a loss of DAM function and some immune pathology, where closer examination of CSF1R-normalized microglial proteins shows an impaired upregulation of DAM-related proteins, and increases in peri-plaque P2RX7 in O_3-exposed mice (Supplementary Fig. 4B), which has been shown to exacerbate AD-like pathology in rodents.[51] Together, the data indicate that the CNS effects of O_3 are determined in part by the spatial localization to amyloid plaques, where O_3 augments protein markers of damage and dysregulates protein markers of the DAM phenotype in the peri-plaque space.

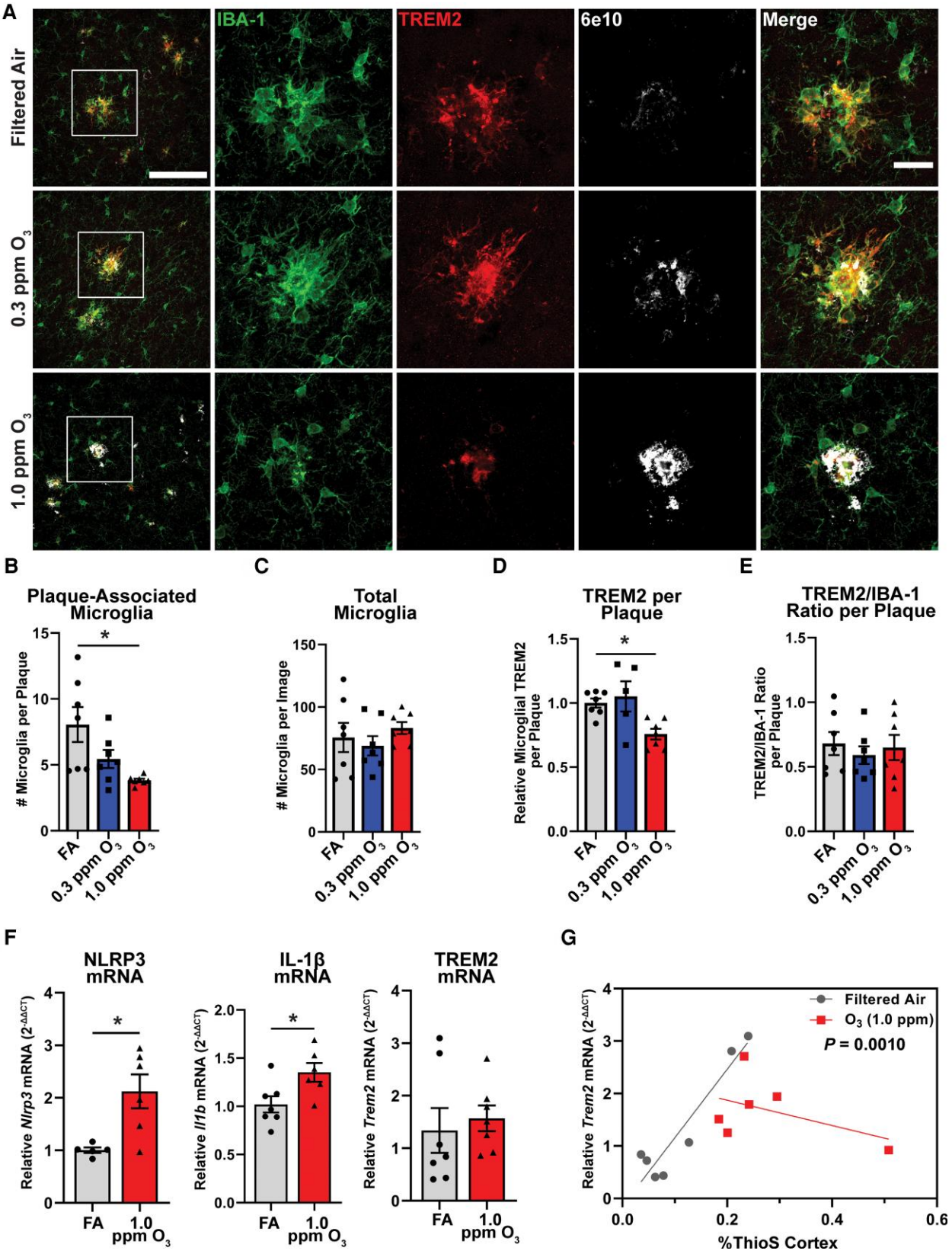

Figure 1 Ozone impairs microglial-plaque association and TREM2 on plaque-associated microglia. 5xFAD mice (10–11 weeks old) were exposed to O_3 (0.3 or 1.0 ppm) or FA by inhalation for 13 weeks. (**A**) Representative confocal images of TREM2 (red), IBA1 (green) and 6e10 (white) in the cortex of 5xFAD mice exposed to O_3 or FA control. Scale bars = 100 μm; *Inset* = 25 μm. (**B** and **C**) Number of (**B**) plaque-associated microglia and (**C**) total microglia per image. (**D** and **E**) Quantification of (**D**) microglial TREM2 relative to plaque area and (**E**) the ratio microglial TREM2 to IBA-1. (**F**) RT-qPCR of the pro-inflammatory genes *Nlrp3 and Il1b* as well as *Trem2* in the cortex of O_3 exposed mice. (**G**) Correlation of %ThioS in the cortex and *Trem2* mRNA. Data are represented as mean ± SEM, $n = 5–7$ mice/exposure group. *$P < 0.05$; one-way ANOVA, Bonferroni *post hoc* or Welch's *t*-test.

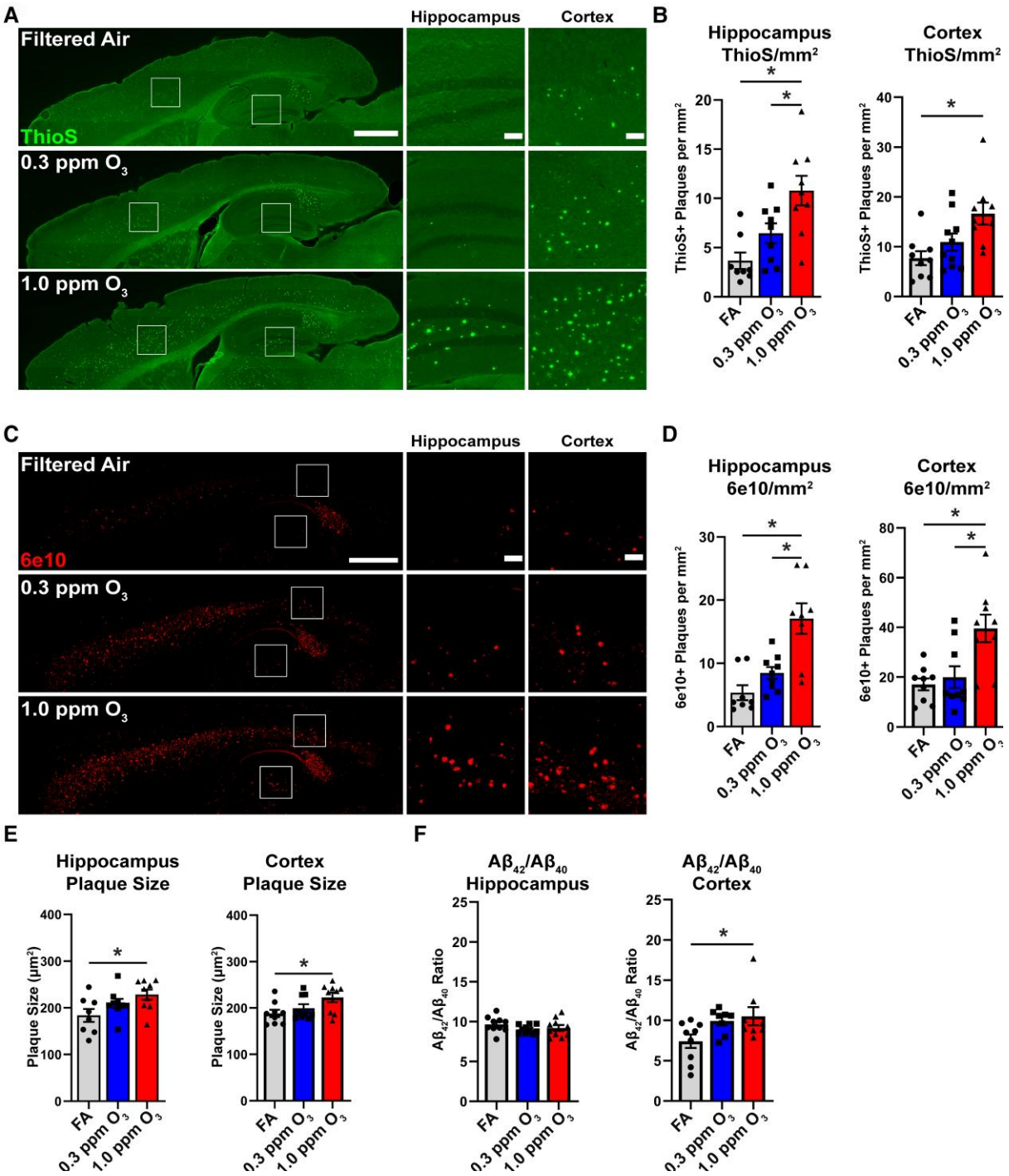

Figure 2 Ozone exposure exacerbates amyloid pathology in 5xFAD mice. 5xFAD mice (10–11 weeks old) were exposed to O_3 (0.3 or 1.0 ppm) or FA by inhalation for 13 weeks. (**A**) Representative images of ThioS+ plaques in the cortex and hippocampus. Scale bars = 1000 µm; *Inset* = 100 µm. (**B**) Quantification of the number of ThioS+ plaques per mm2 in the hippocampus and cortex. (**C**) Representative images of 6e10+ Aβ in the cortex and hippocampus. Scale bars = 1000 µm; *Inset* = 100 µm. (**D**) Quantification of the number of 6e10+ plaques per mm^2 in the hippocampus and cortex. (**E**) Quantification of the average size of 6e10+ plaques in the hippocampus and cortex. (**F**) The ratio of DEA soluble $A\beta_{42}$ to $A\beta_{40}$ in the hippocampus and cortex. Data are represented as mean ± SEM, $n = 8$–10 mice/exposure group. *$P < 0.05$, one-way ANOVA, Bonferroni *post hoc*.

Ongoing Alzheimer's disease neuropathology augments the pulmonary and circulating factor response to ozone

We next sought to understand the peripheral immune response of 5xFAD and control (WT) mice to O_3. Examination of the bronchoalveolar lavage (BAL) in O_3 exposed mice showed an increase in the total cells, macrophages, neutrophils and eosinophils in 5xFAD mice exposed to 1.0 ppm O_3, but not WT mice (Fig. 5A). Analysis of total protein concentration in the BAL fluid showed an increase in both mouse strains in the 1.0 ppm O_3 exposed groups, but no genotype differences (Fig. 5B), suggesting that 5xFAD mice

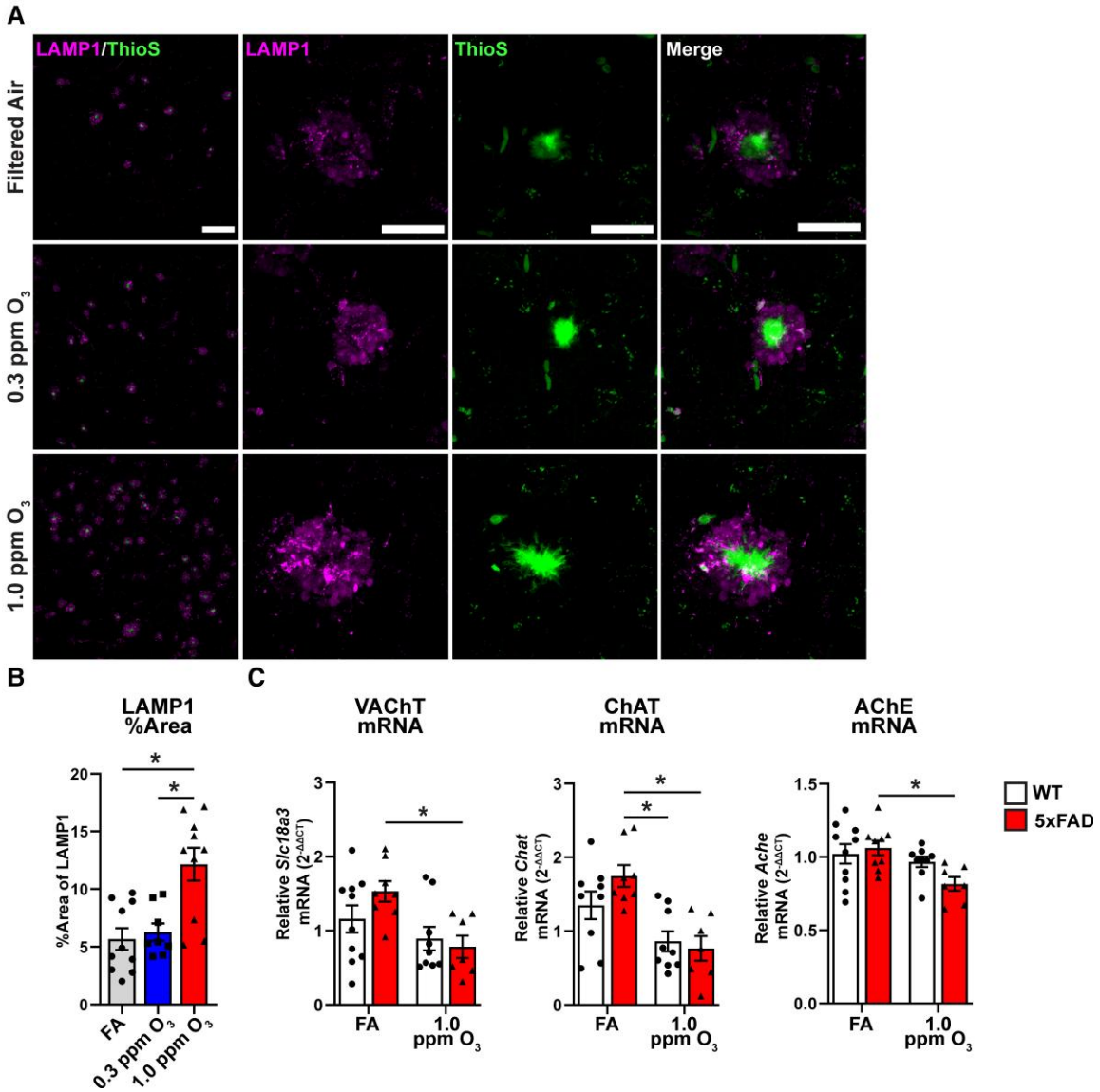

Figure 3 Ozone exposure exacerbates neuritic dystrophy and dysregulates acetylcholinergic gene expression. 5xFAD mice (10–11 weeks old) were exposed to O_3 (0.3 or 1.0 ppm) or FA by inhalation for 13 weeks. (**A**) Representative confocal images of ThioS (green) and LAMP1 (magenta) taken at ×20 (*top*) or ×63 (*bottom*) in the M1/M2 cortex of 5xFAD mice exposed to O_3. Scale bars: *top* = 100 µm; *bottom* = 25 µm. (**B**) Quantification of LAMP1 per cent area. (**C**) mRNA expression of *Slc18a3* (VAChT), *Chat* and *Ache* in the cortex of O_3 exposed 5xFAD and WT mice. $n = 8$–10 mice/exposure group. *$P < 0.05$; one-way ANOVA, Bonferroni *post hoc* or Welch's *t*-test.

have augmented immune cell infiltration into the alveolar compartment in response to O_3, but no differences in pulmonary damage.

In order to exclude aberrant transgene expression in peripheral tissues of 5xFAD mice as the cause of these pulmonary differences, we examined human APP (hAPP) expression in the brain and lung of control and 5xFAD mice (Supplementary Fig. 5A and B), where hAPP expression was only noted in the brains of the 5xFAD transgenic mice. As such, 5xFAD differences in the peripheral measures produced in response to O_3 were attributed to the peripheral consequences of the ongoing AD neuropathology. Further, given that the transgenes in the 5xFAD mouse model are inserted under a neuronal specific element of the *Thy1* promoter,[27] it is unlikely that extra-CNS expression of transgenes is driving this effect.

Given the alterations in immune cell infiltration into the lungs of 5xFAD mice, we next aimed to understand the molecular underpinnings of these differences. Using NanoString mRNA panels, we examined the transcriptomic signatures of the isolated BAL immune cells from FA- and 1.0 ppm O_3-exposed mice (Fig. 5C–E). Volcano plots showing the differences in gene expression of BAL immune cells compared to FA control demonstrate a unique transcriptional profile in O_3-exposed 5xFAD mice, including genes related to immune cell chemotaxis, such as *Cxcr2*, and interestingly, *Trem2* (Fig. 5C). Undirected pathway analysis of 5xFAD versus WT O_3 exposure shows broad perturbations in pathways related to cytokine signalling and chemotaxis (Fig. 5D), further confirming that 5xFAD mice have an augmented pulmonary immune response. Analysis of specific gene sets shows increased expression in multiple chemokines and cytokines, as well as key endothelial cell markers (Fig. 5E) in O_3-exposed 5xFAD compared to WT mice. Taken together, these analyses demonstrate broad changes in the 5xFAD pulmonary immune response without aberrant transgene

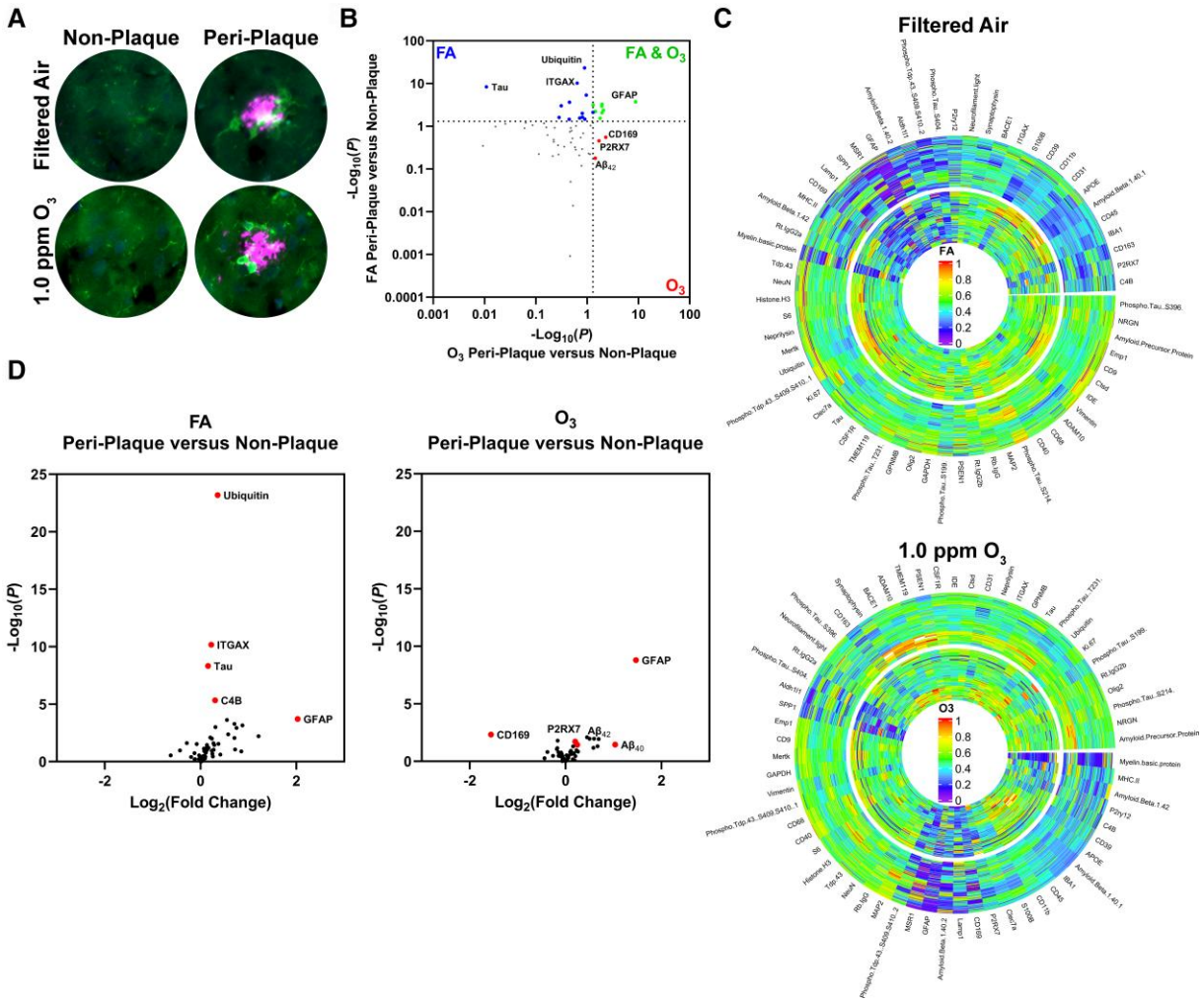

Figure 4 O_3 alters the peri-plaque microenvironment and dysregulates key DAM proteins. 5xFAD mice (10–11 weeks old) were exposed to O_3 (0.3 or 1.0 ppm) or FA by inhalation for 13 weeks. (**A**) Representative images from NanoString GeoMX DSP platform of IBA-1 (green) and Aβ (magenta) in the cortex of 5xFAD mice. (**B**) Plot comparing changes from peri-plaque to non-plaque areas in FA and O_3. (**C**) Radial heat map of protein changes from non-plaque (*outer circle*) to peri-plaque (*inner circle*) regions in O_3 exposed 5xFAD mice. (**D**) Volcano plots comparing peri-plaque versus non-plaque areas for FA and O_3. $n = 4$ mice/group (34–36 peri-plaque and 36 plaque-distant ROIs per mouse).

expression, suggesting that ongoing AD pathology may impact pulmonary immune responses.

Peripheral HMGB1 regulates O_3-induced CNS change

In our next approach, we aimed to understand what circulating factors may be contributing to the CNS effects of O_3. We previously found that canonical cytokines and chemokines are not upregulated in response to O_3 exposure in rodents.[24] Examination of serum by ELISA and array showed an increase in three serum proteins (HMGB1, IL-9, VEGF) in only the 5xFAD mice in response to O_3 (Fig. 6A), but not WT mice (Supplementary Fig. 6), further confirming a combinatorial effect of O_3 exposure and ongoing AD pathology in peripheral immune responses.

To verify the CNS consequences of circulating HMGB1 and begin to understand the functional impact of increased serum HMGB1 on CNS changes in response to air pollution, we injected recombinant HMGB1 (rHMGB1, 32.5 μg) into mice by tail vein, a dose previously identified in experiments with LPS-treated animals.[52] At 3 h, rHMGB1 injection decreased mRNA expression of VAChT and ChAT in the cortex (Fig. 6B), but no changes were seen in AChE mRNA expression (data not shown). Next, we examined whether rHMGB1 impacted *Trem2* mRNA expression. While no significant changes were seen in *Trem2* expression in the cortex, rHMGB1 significantly impaired *Trem2* expression in the midbrain (Fig. 6C), a region that has been previously shown to be particularly sensitive to the effects of air pollution and circulating signal-induced neuroinflammation.[11] We did not observe changes in microglial morphology at this dose and timepoint of rHMGB1 injection, further pointing to the complicated nature of the peripheral aberrations in O_3-induced CNS changes (Supplementary Fig. 7A and B). To further investigate the role of peripheral HMGB1 on O_3-induced CNS changes, we utilized a cre-lox system to create a myeloid-specific knockout of HMGB1. *Hmgb1*$^{fl/fl}$*LysM*-cre^{+} mice showed robust reduction in expression of *Hmgb1* in only peripheral myeloid cell populations (intraperitoneal macrophages and alveolar macrophages) without a change in brain or microglial *Hmgb1* expression or number of microglia (Supplementary Fig. 8A and B), supporting that HMGB1 is specifically knocked down in peripheral myeloid populations. Short term O_3 exposure in *Hmgb1*$^{fl/fl}$*LysM*-cre^{-} mice

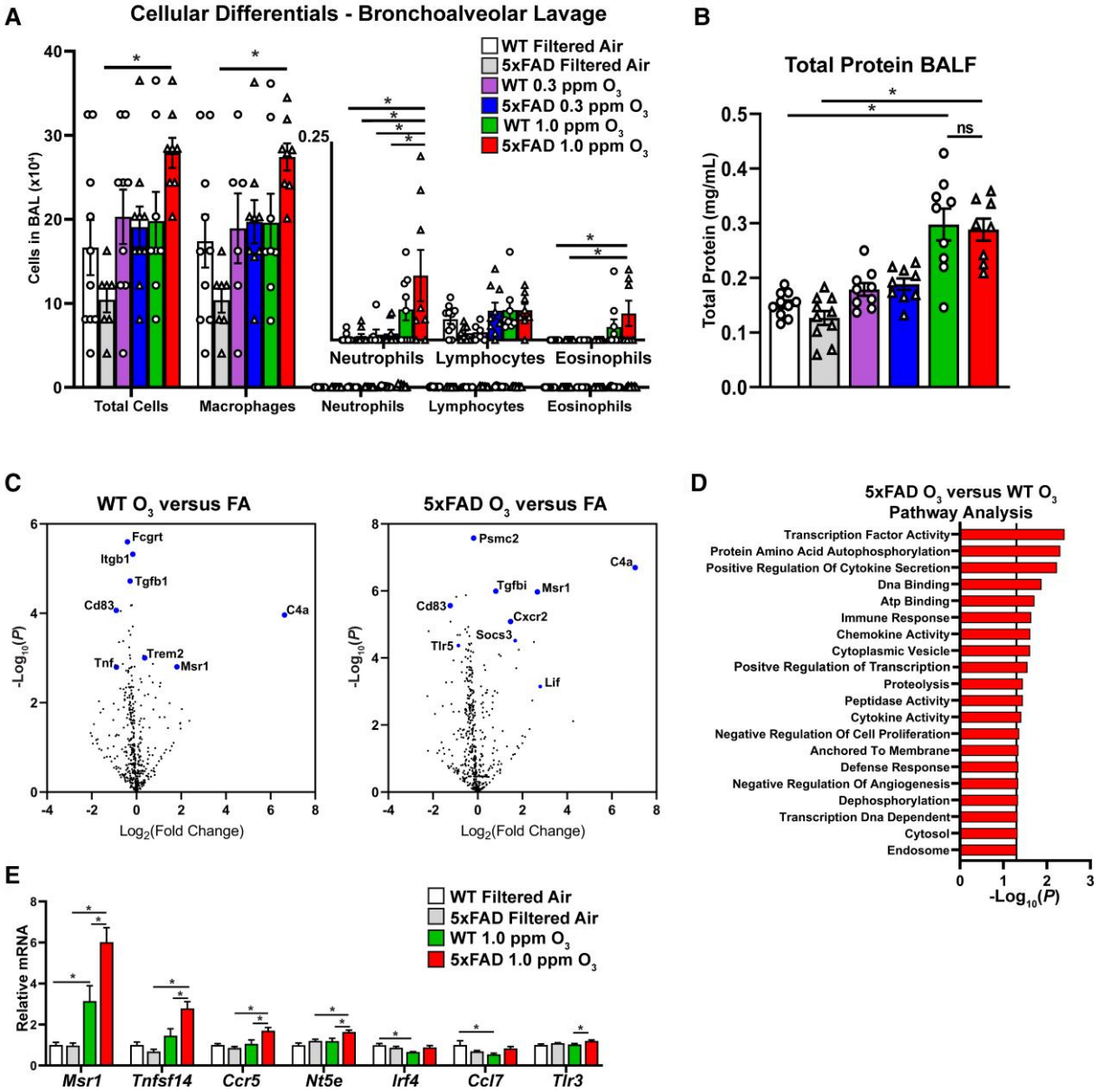

Figure 5 Ongoing AD pathology augments pulmonary and peripheral immune responses to O_3. 5xFAD mice (10–11 weeks old) were exposed to O_3 (0.3 or 1.0 ppm) or FA by inhalation for 13 weeks. (**A**) Cellular differentials from bronchoalveolar lavage (BAL) from O_3-exposed 5xFAD and control littermates. (**B**) Total protein in BAL fluid. (**C**) Volcano plots from NanoString analysis of BAL cells from O_3 WT versus FA and O_3 5xFAD versus FA. Highlighted genes represent a subset of significantly changed genes after FDR correction (Benjamani-Hochberg, $P < 0.01$). (**D**) Undirected pathway analysis of 5xFAD O_3 versus WT O_3 showing the top 20 significantly changed pathways ($P < 0.05$). (**E**) Analysis of gene changes between 5xFAD and WT mice exposed to O_3.

showed a decrease in *Trem2* expression in the cortex and midbrain (Fig. 6D), an increase in *Nlrp3* in the midbrain (Fig. 6E), and no changes in *Il1b* (data not shown), but these effects were abolished in *Hmgb1*$^{fl/fl}$*LysM*-cre^{+} mice (Fig. 6D and E), further implicating peripheral myeloid HMGB1 in O_3-induced CNS changes. Lastly, we observed that neither HMGB1 mRNA or protein expression in the cortex of 5xFAD mice exposed to O_3 was changed (Supplementary Fig. 9A and B), suggesting that peripheral HMGB1, and not CNS-derived HMGB1 likely plays a more important role in O_3-indcued CNS changes. These findings support that O_3exposure induces circulating factors, such as HMGB1, that may regulate O_3-induced CNS pathology.

Discussion

Epidemiological studies have increasingly associated air pollution exposure with increased risk of AD, cognitive decline, and dementia,[22,23,53,54] but how urban air pollution augments amyloid plaque deposition and elevates AD risk is a source of debate and is likely due to multiple interacting mechanisms. Here, we began to outline the role of the lung-brain-axis in amyloid pathology using O_3, a reactive gas air pollutant associated with AD risk and cognitive decline.[4,22,23] that is unable to translocate to the CNS parenchyma to exert effects.[20,21] O_3 was shown to augment amyloid pathology in a pattern that was consistent with loss of TREM2 function, including impaired upregulation of TREM2 expression, attenuated microglial

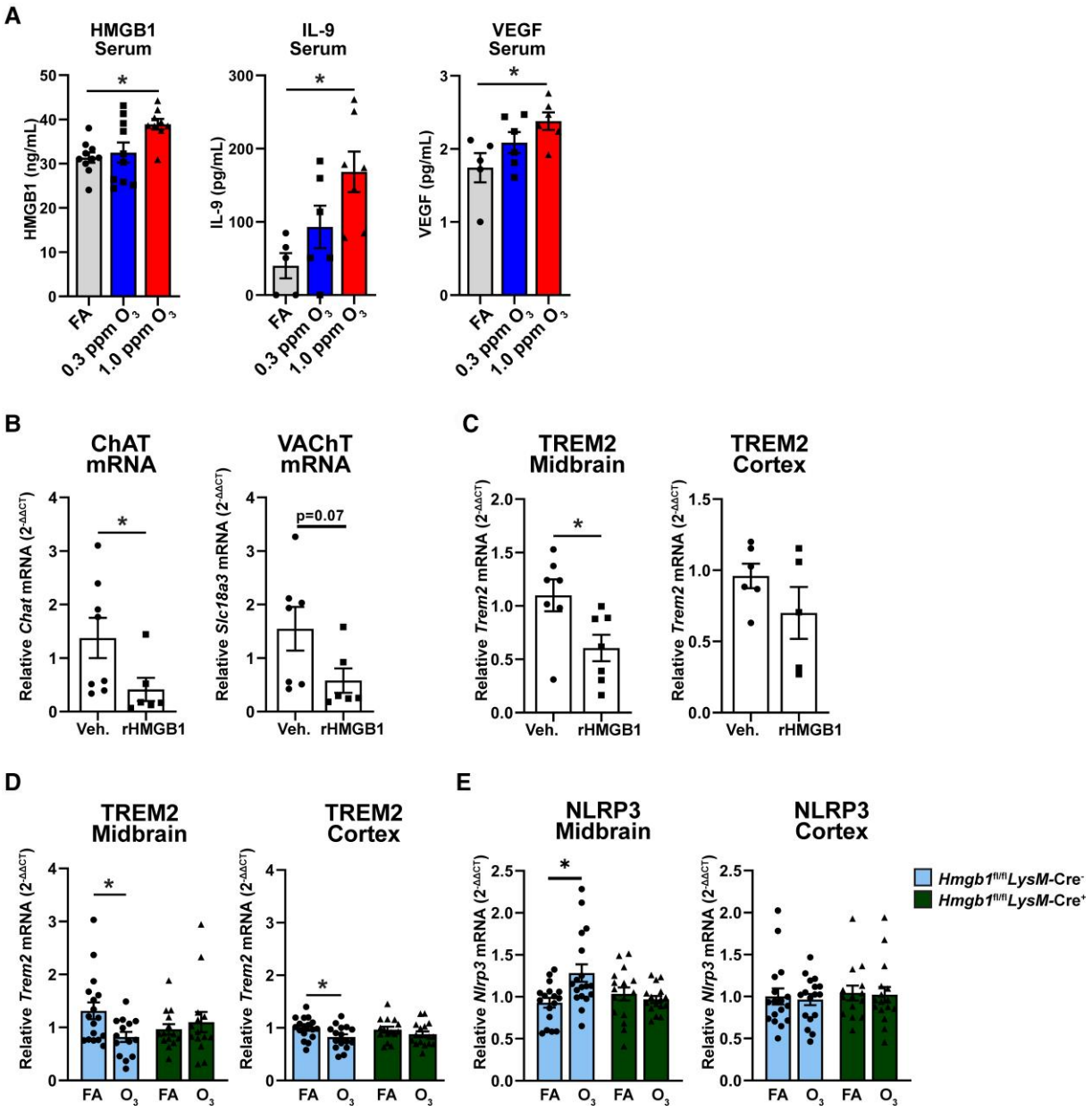

Figure 6 Peripheral HMGB1 regulates O_3-induced CNS changes. 5xFAD mice (10–11 weeks old) were exposed to O_3 (0.3 or 1.0 ppm) or FA by inhalation for 13 weeks. (**A**) Serum analysis of HMGB1, IL-9, and VEGF in 5xFAD mice exposed to O_3. C57Bl/6 mice were injected with rHMGB1 (32.5 μg) or vehicle (Veh.) by tail and samples were collected 3 h after injection (**B**) mRNA analysis of acetylcholinergic genes in mice injected with rHMGB1. (**C**) mRNA analysis of *Trem2* in midbrain and cortex of mice injected with rHMGB1. *Hmgb1*$^{fl/fl}$*LysM*-cre$^-$ and *Hmgb1*$^{fl/fl}$*LysM*-cre$^+$were exposed to O_3 (1.0 ppm) or FA for 3 days, 4 h/day. (**D** and **E**) mRNA expression of (**D**) *Trem2* and (**E**) *Nlrp3* in cortex and midbrain of *Hmgb1*$^{fl/fl}$*LysM*-cre$^-$ and *Hmgb1*$^{fl/fl}$LysM-cre$^+$exposed to O_3. $n = 5$–10 mice/exposure group for 13 wk O_3 exposure, $n = 6$–7 mice/treatment group for rHMGB1, $n = 16$–18 mice/exposure group for short term O_3. $^*P < 0.05$; Welch's *t*-test, or one- or two-way ANOVA, Bonferroni *post hoc*.

plaque association, disrupted plaque micro-environment proteomic profiles, enhanced amyloid load, and exacerbated amyloid-associated neuron damage, where the lung-brain axis hypothesis holds that these effects are likely caused by the peripheral consequences of O_3. Consistent with this premise, 5xFAD mice showed elevated circulating factors in response to O_3, including HMGB1, and an enhanced pulmonary immune response that was concurrent with the O_3 augmented amyloid-associated neuropathology. Mechanistically, this work directly tests the role of peripheral HMGB1 as one mechanism out of many, through which O_3 can impact the brain. More specifically, O_3 exposure was shown to elevate circulating HMGB1 in 5xFAD mice; intravenous administration of rHMGB1 in control mice was demonstrated to trigger neuroimmune responses, including impaired TREM2 expression; genetic deletion of peripheral myeloid cell HMGB1 was shown to rescue O_3-induced loss of *Trem2* expression. These findings are the first to reveal that O_3 exposure augments amyloid plaque pathology, and that O_3 does this in a pattern consistent with loss of TREM2 function, where the peripheral responses to O_3, such as HMGB1, can mediate TREM2 disruption. Unexpectedly, given the enhanced pulmonary immune sensitivity of 5xFAD mice to O_3exposure, these findings also support that the lung-brain axis is bidirectional, where ongoing neuron damage

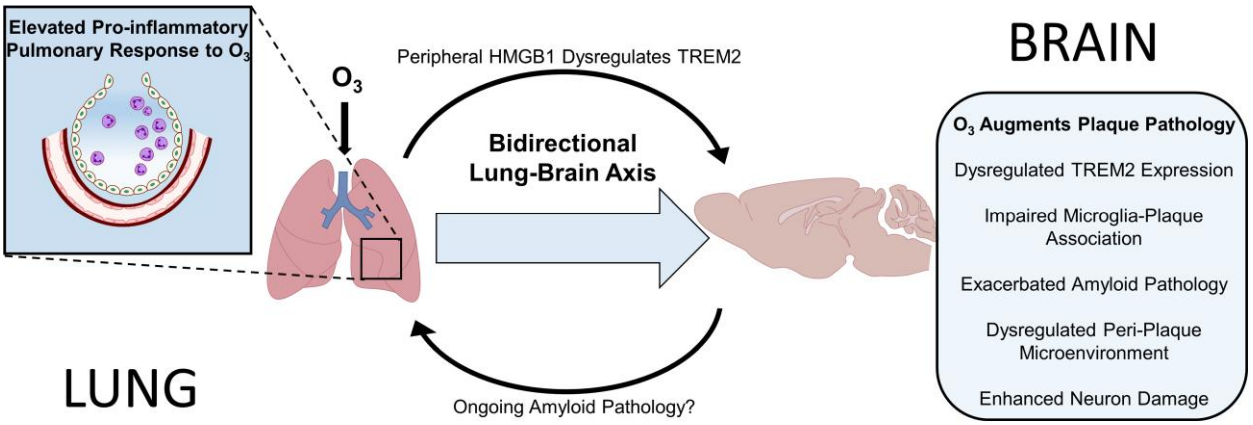

Figure 7 O_3 regulates the amyloid plaque micro-environment through the bidirectional lung-brain axis. Exposure to O_3, a reactive air pollutant unable to translocate to the brain to exert CNS effects, caused: reduced microglial-plaque association, impaired CNS *Trem2* upregulation in response to plaques, exacerbated amyloid and neuronal pathology, and dysregulated the peri-plaque microenvironment in 5xFAD mice, effects commonly associated with loss of TREM2 function. 5xFAD mice also exhibited enhanced circulating factors (HMGB1), elevated pulmonary immune cell trafficking, and an augmented pulmonary immune cell pro-inflammatory transcriptome in response to O_3, when compared to control mice, supporting a role for ongoing Aβ neuropathology in the pulmonary response to air pollution, revealing a bi-directional lung-brain axis governing central and peripheral immune responses. Mechanistically, iv injection of recombinant HMGB1 in control mice impaired brain *Trem2* expression and genetic ablation of HMGB1 in peripheral myeloid cells abolished O_3-induced reduction of TREM2, revealing a role for peripheral HMGB1 in the regulation of CNS *Trem2* expression. These findings implicate urban air pollution, the periphery, and the lung-brain axis in amyloid pathology and highlight the potential role of TREM2 and HMGB1 in this process, identifying novel potential therapeutic targets for the regulation of CNS *Trem2* expression and Alzheimer's disease.

may also regulate the pulmonary immune response to urban air pollution (Fig. 7).

There is increasing interest in the underlying mechanisms regulating how urban air pollution can affect the brain,[55] and most animal and *in vitro* studies have focused on direct toxicity mechanisms,[9,56] where components of air pollution translocate into the CNS to directly exert neurotoxic and pro-inflammatory effects. While certainly true for some components of air pollution, such as metals,[57] this mechanism falls short for gaseous components of air pollution that are unable to pass the respiratory barrier, such as O_3, which are compositionally prevalent and also linked with an increased risk of AD.[4,53] The lung-brain axis hypothesis holds that the pulmonary immune response and consequent systemic signals, such as cells and circulating factors, regulate CNS health and disease.[24] Consistent with this, we have previously shown that O_3 results in a persistent neuroimmune response, likely due to circulating factors, which was hypothesized to be caused by the peripheral immune response.[24] This is further supported by other reports identifying changes in the peripheral immune response, circulating factors, and the neuroimmune response to O_3. [24,58,59] Here, we demonstrated that the lung-brain axis effects of O_3 exposure include impaired microglial-plaque association (Fig. 1), neuroinflammation (Fig. 1), increased amyloid neuropathology (Fig. 2), and neuritic dystrophy (Fig. 3). Importantly, the data revealed an uncoupling of the *Trem2*-plaque response and a decrease in the levels of TREM2 around the plaque, despite no evidence that the plaque-associated microglia TREM2 expression levels were changed (Fig. 1). We next determined the consequences of subchronic O_3 exposure at the level of the peri-plaque microenvironment, where we show dysregulated protein expression of key DAM proteins, increased Aβ processing enzymes, elevated phosphorylated-tau, and augmented many other protein markers of pathology (Fig. 4). Interestingly, this O_3-induced amyloid neuropathology phenotype is consistent to what occurs with loss of TREM2 function in 5xFAD mice,[19,46] which further suggests that O_3 may be regulating CNS effects through dysregulated TREM2 expression or function.

DAM cells surround and clear plaques through a transcriptomic shift regulated by TREM2,[18,45] and studies indicate that loss of TREM2 exacerbates amyloid pathology, particularly in late stages of disease.[19,46] While we previously have shown that air pollution exposure impaired TREM2 expression and DAM genes,[40] the impact of air pollution exposure on microglial-plaque association has not been studied. Here, we show that O_3 exposure impaired microglial-plaque association (Fig. 1), which is the first evidence that air pollution may alter AD neuropathology through an impaired microglial clearance pathways. We hypothesized that O_3-impaired microglia-plaque association may be due to impaired TREM2 expression. While TREM2 expression was decreased around plaques, this was attributable to the decreased number of microglia around the plaques, suggesting a more complicated mechanism than an impaired expression of TREM2. This apparent lack of TREM2 expression change in microglia may be due to the limitations of imaging modalities used or changes in TREM2 function and processing that were unable to be investigated in this study. However, we observed an uncoupling of plaque increased *Trem2* expression, suggesting that O_3 exposure may still be impacting this response from microglia. Taken together, these data point to a central role for microglia in air pollution-altered AD-like pathology.

The neuropathology of AD is dependent on the plaque microenvironment,[43] and in the current study, we discovered that spatial resolution and plaque proximity are important for understanding how O_3 affects the brain. We found that O_3 dysregulated both the peri-plaque micro-environment and plaque-distant regions (Fig. 4). Importantly, data revealed a dysregulated shift in the plaque-distant to peri-plaque micro-environments, where plaque-distant regions were similar to peri-plaque regions after O_3 exposure, suggesting that air pollution may exacerbate AD pathology through multiple mechanisms at the level of the plaque microenvironment (Fig. 4). Further, several damage and inflammatory proteins had reached a ceiling effect in the plaque-distant regions of the O_3 exposed brains, suggesting that O_3 may also impact plaque-distant areas and result in multiple insults that microglia respond to. As such, we propose that the concurrent insults of amyloid pathology and O_3-induced CNS effects may overwhelm microglial ability to efficiently respond to and clear plaques.

Taken together, these findings demonstrate that O_3 exposure alters the peri-plaque micro-environment, which offers a previously unexplored level of spatial and quantitative resolution into how air pollution may be regulating key pathological mechanisms in AD.

Previous research exploring the lung-brain axis has investigated how the pulmonary response to air pollutants affect the brain.[24] Here, we demonstrate that the lung-brain axis of air pollution is bidirectional, where ongoing amyloid pathology enhances sensitivity to the pulmonary immune response to O_3. While we did not investigate the underlying mechanism behind the increased immune sensitivity, there are several possible mechanisms including alterations in neuronal signalling to the lung, changes in circulating immune cells, or complex peripheral immune interactions involving other organs systems such as the spleen or liver. These findings are consistent with other CNS insults, where it has been known that stroke dysregulates the peripheral immune system and can lead to a higher susceptibility to pneumonia and pulmonary infection through peripheral immunodepression.[60] As such, our data add to the growing body of evidence that indicates that CNS disease affects the peripheral immune response. We also identified HMGB1, IL-9, and VEGF as potential contributors along the lung-brain axis, and HMGB1 was shown separately to regulate O_3-induced CNS gene expression changes (Fig. 6). Together, these data support that ongoing AD pathology augments the pulmonary immune response to air pollution, and that peripheral circulating factors, such as HMGB1, regulate the lung-brain axis. It has been observed that patients with isolated traumatic brain injury can spontaneously develop acute lung injury,[61] and the mechanisms underlying communication between lung and brain pathology is urgently relevant given reports of cognitive symptoms in patients with or recovering from COVID-19.[62–64] However, little is mechanistically known about the communication between lung and brain disease, and these data may have implications reaching far beyond air pollution-induced lung damage and AD.

In conclusion, here we identify a robust exacerbation of amyloid pathology in response to O_3 exposure consistent with reports of increased amyloid pathology in humans exposed to ambient air pollution.[7] Further, we show a novel mechanism, where O_3 exposure impairs the ability of microglia to associate with amyloid plaques and uncouples *Trem2* upregulation with increasing plaque load, indicating that air pollution may exacerbate AD pathology primarily through impaired mechanisms of plaque restriction. We found that this decrease in microglial-plaque association exacerbated neuritic dystrophy and decreased expression of components of the acetylcholinergic system, one of the primary symptomatic targets in AD. Further, we show that O_3 exacerbates pathology in both the peri-plaque microenvironment, as well as plaque-distant environment and dysregulates proteins associated with the plaque-clearing DAM phenotype. Surprisingly, in the lung, we found augmented immune cell infiltration in 5xFAD mice only, suggesting that ongoing AD pathology may augment peripheral immune response. Further transcriptomic investigation suggested that ongoing AD pathology may exacerbate the chemotactic responses in the periphery and augment the pro-inflammatory pulmonary immune profile in response to air pollution. The 5xFAD humoral response to O_3 was also enhanced, where O_3 upregulated circulating HMGB1 in only 5xFAD mice. Additional experiments revealed that peripheral HMGB1 regulates CNS *Trem2* expression, highlighting a role for the periphery in the DAM phenotype. We speculate that the bidirectional aspect of the lung-brain axis may be driven by crosstalk between the CNS immune system and the peripheral immune system, where ongoing neurodegenerative pathology could lead to a primed immune state outside of the brain, perhaps through breakdown of CNS barriers leading to increased exposure of pro-inflammatory components of neurodegenerative pathology. Interestingly, this suggests that some of the peripheral markers of AD neuropathology could ultimately play a role, including neuronal contributions, emphasizing the importance of further research inquiry. These findings have implications for AD and pulmonary comorbidities such as COPD, asthma, and acute respiratory distress syndrome (ARDS). How air pollution inhalation impacts AD pathology has been a critical question in the field for many years, and here we show that O_3 exacerbates amyloid pathology at the level of the peri-plaque microenvironment and the lung-brain axis, where HMGB1 may be one of the peripheral factors that regulate the CNS (Fig. 7). We believe these findings provide much needed insight into the potential aetiology and pathobiology of AD and identify the lung-brain axis as a potential target for therapeutic intervention. Future studies defining the types of air pollution exposure culpable and the necessary pulmonary response to impact AD neuropathology will be critical advances to the field.

Acknowledgements

The authors would like to thank all members of the Block Lab, Oblak Lab, and Landreth lab for their thoughtful discussions and technical support. The authors would also like to thank Dr Mark Higuchi for the generous gift of the Hinners exposure chambers and John McKee for his expertise and assistance in setting up and validating the O_3 exposure system. All authors thank the Multiplex Analysis Core at the Indiana University Melvin and Bren Simon Cancer Center for providing support in analysing samples and interpretation of data, Christopher Llyod and Deborah Baker for their technical support with staining protocols and microscopy, and Andy Tsai and Peter Bor-Chian Lin for their technical assistance with NanoString instrumentation. The research described in this article has been reviewed by the Center Public Health and Environmental Assessment, US Environmental Protection Agency and approved for publication. Approval does not signify that the contents necessarily reflect the views and the policies of the Agency nor does mention of trade names or commercial products constitute endorsement or recommendation for use. The contents do not reflect the views of the US Department of Veteran's Affairs nor the United States Government.

Funding

This study was graciously funded by VA Merit Award I01 BX004161 and supported by the NIH RO1 ES029835GW and NIH R01 ES028104 awarded to M.L.B.

Competing interests

The authors report no competing interests.

Supplementary material

Supplementary material is available at *Brain* online.

References

1. Nichols E, Steinmetz JD, Vollset SE, *et al*. Estimation of the global prevalence of dementia in 2019 and forecasted prevalence in

2050: an analysis for the Global Burden of Disease Study 2019. *Lancet Public Health*. 2022;7(2):e105–e125.
2. Long JM, Holtzman DM. Alzheimer disease: An update on pathobiology and treatment strategies. *Cell*. 2019;179(2):312–339.
3. Jayaraj RL, Rodriguez EA, Wang Y, Block ML. Outdoor ambient air pollution and neurodegenerative diseases: The neuroinflammation hypothesis. *Curr Environ Health Rep*. 2017;4(2):166–179.
4. Croze ML, Zimmer L. Ozone atmospheric pollution and Alzheimer's disease: From epidemiological facts to molecular mechanisms. *J Alzheimer's Dis*. 2018;62:503–522.
5. Kilian J, Kitazawa M. The emerging risk of exposure to air pollution on cognitive decline and Alzheimer's disease – Evidence from epidemiological and animal studies. *Biomed J*. 2018;41(3):141–162.
6. Karran E, Mercken M, De Strooper B. The amyloid cascade hypothesis for Alzheimer's disease: an appraisal for the development of therapeutics. *Nat Rev Drug Discov*. 2011;10(9):698–712.
7. Iaccarino L, La Joie R, Lesman-Segev OH, *et al*. Association between ambient air pollution and amyloid positron emission tomography positivity in older adults with cognitive impairment. *JAMA Neurol*. 2020;78:197–207.
8. Akhter H, Ballinger C, Liu N, van Groen T, Postlethwait EM, Liu R-M. Cyclic ozone exposure induces gender-dependent neuropathology and memory decline in an animal model of Alzheimer's disease. *Toxicol Sci*. 2015;147(1):222–234.
9. Cacciottolo M, Wang X, Driscoll I, *et al*. Particulate air pollutants, APOE alleles and their contributions to cognitive impairment in older women and to amyloidogenesis in experimental models. *Transl Psychiatry*. 2017;7(1):e1022.
10. Hullmann M, Albrecht C, van Berlo D, *et al*. Diesel engine exhaust accelerates plaque formation in a mouse model of Alzheimer's disease. *Part Fibre Toxicol*. 2017;14(1):35.
11. Levesque S, Taetzsch T, Lull ME, *et al*. Diesel exhaust activates and primes microglia: Air pollution, neuroinflammation, and regulation of dopaminergic neurotoxicity. *Environ Health Perspect*. 2011;119(8):1149–1155.
12. Roqué PJ, Dao K, Costa LG. Microglia mediate diesel exhaust particle-induced cerebellar neuronal toxicity through neuroinflammatory mechanisms. *NeuroToxicology*. 2016;56:204–214.
13. Bolton JL, Marinero S, Hassanzadeh T, *et al*. Gestational exposure to air pollution alters cortical volume, microglial morphology, and microglia-neuron interactions in a sex-specific manner. *Front Synaptic Neurosci*. 2017;9:10.
14. Morris-Schaffer K, Merrill AK, Wong C, Jew K, Sobolewski M, Cory-Slechta DA. Limited developmental neurotoxicity from neonatal inhalation exposure to diesel exhaust particles in C57BL/6 mice. *Part Fibre Toxicol*. 2019;16(1):1.
15. Heneka MT, Carson MJ, Khoury JE, *et al*. Neuroinflammation in Alzheimer's disease. *Lancet Neurol*. 2015;14(4):388–405.
16. Wang Y, Ulland TK, Ulrich JD, *et al*. TREM2-mediated early microglial response limits diffusion and toxicity of amyloid plaques. *J Exp Med*. 2016;213(5):667–675.
17. Reed-Geaghan EG, Croxford AL, Becher B, Landreth GE. Plaque-associated myeloid cells derive from resident microglia in an Alzheimer's disease model. *J Exp Med*. 2020;217(4).
18. Keren-Shaul H, Spinrad A, Weiner A, *et al*. A unique microglia type associated with restricting development of Alzheimer's disease. *Cell*. 2017;169(7):1276–1290.e17.
19. Jay TR, Hirsch AM, Broihier ML, *et al*. Disease progression-dependent effects of TREM2 deficiency in a mouse model of Alzheimer's disease. *J Neurosci*. 2017;37(3):637.
20. Pryor WA, Squadrito GL, Friedman M. A new mechanism for the toxicity of ozone. *Toxicol Lett*. 1995;82-83:287–293.
21. Frampton MW, Pryor WA, Cueto R, Cox C, Morrow PE, Utell MJ. Ozone exposure increases aldehydes in epithelial lining fluid in human lung. *Am J Respir Crit Care Med*. 1999;159(4 Pt 1):1134–1137.
22. Jung CR, Lin YT, Hwang BF. Ozone, particulate matter, and newly diagnosed Alzheimer's disease: a population-based cohort study in Taiwan. *J Alzheimers Dis*. 2015;44(2):573–584.
23. Cleary EG, Cifuentes M, Grinstein G, Brugge D, Shea TB. Association of low-level ozone with cognitive decline in older adults. *J Alzheimer's Dis: JAD*. 2018;61(1):67–78.
24. Mumaw CL, Levesque S, McGraw C, *et al*. Microglial priming through the lung-brain axis: the role of air pollution-induced circulating factors. *FASEB J*. 2016;30(5):1880–1891.
25. Erickson MA, Jude J, Zhao H, *et al*. Serum amyloid A: an ozone-induced circulating factor with potentially important functions in the lung-brain axis. *FASEB J*. 2017;31(9):3950–3965.
26. Rusanen M, Ngandu T, Laatikainen T, Tuomilehto J, Soininen H, Kivipelto M. Chronic obstructive pulmonary disease and asthma and the risk of mild cognitive impairment and dementia: a population based CAIDE study. *Curr Alzheimer Res*. 2013;10(5):549–555.
27. Oakley H, Cole SL, Logan S, *et al*. Intraneuronal β-amyloid aggregates, neurodegeneration, and neuron loss in transgenic mice with five familial Alzheimer's disease mutations: Potential factors in amyloid plaque formation. *J Neurosci*. 2006;26(40):10129–10140.
28. Maarouf CL, Kokjohn TA, Whiteside CM, *et al*. Molecular differences and similarities between Alzheimer's disease and the 5XFAD transgenic mouse model of amyloidosis. *Biochem Insights*. 2013;6:BCI.S13025.
29. Bundy JL, Vied C, Badger C, Nowakowski RS. Sex-biased hippocampal pathology in the 5XFAD mouse model of Alzheimer's disease: A multi-omic analysis. *J Comp Neurol*. 2019;527(2):462–475.
30. Sadleir KR, Eimer WA, Cole SL, Vassar R. Aβ reduction in BACE1 heterozygous null 5XFAD mice is associated with transgenic APP level. *Mol Neurodegener*. 2015;10:1.
31. Sadleir KR, Popovic J, Vassar R. ER stress is not elevated in the 5XFAD mouse model of Alzheimer's disease. *J Biol Chem*. 2018;293(48):18434–18443.
32. Yanai H, Matsuda A, An J, *et al*. Conditional ablation of HMGB1 in mice reveals its protective function against endotoxemia and bacterial infection. *Proc Natl Acad Sci*. 2013;110(51):20699–20704.
33. Plopper CG, Hyde DM. The non-human primate as a model for studying COPD and asthma. *Pulm Pharmacol Ther*. 2008;21(5):755–766.
34. Hatch GE, Slade R, Harris LP, *et al*. Ozone dose and effect in humans and rats. A comparison using oxygen-18 labeling and bronchoalveolar lavage. *Am J Respir Crit Care Med*. 1994;150(3):676–683.
35. Ballinger CA, Cueto R, Squadrito G, *et al*. Antioxidant-mediated augmentation of ozone-induced membrane oxidation. *Free Radic Biol Med*. 2005;38(4):515–526.
36. Miller DB, Snow SJ, Henriquez A, *et al*. Systemic metabolic derangement, pulmonary effects, and insulin insufficiency following subchronic ozone exposure in rats. *Toxicol Appl Pharmacol*. 2016;306:47–57.
37. Snow SJ, Gordon CJ, Bass VL, *et al*. Age-related differences in pulmonary effects of acute and subchronic episodic ozone exposures in Brown Norway rats. *Inhal Toxicol*. 2016;28(7):313–323.
38. Itah R, Gitelman I, Davis C. A replacement for methoxyflurane (Metofane) in open-circuit anaesthesia. *Lab Animals*. 2004;38(3):280–285.
39. Nagate T, Chino T, Nishiyama C, *et al*. Diluted isoflurane as a suitable alternative for diethyl ether for rat anaesthesia in regular toxicology studies. *J Vet Med Sci*. 2007;69(11):1137–1143.

40. Greve HJ, Mumaw CL, Messenger EJ, *et al*. Diesel exhaust impairs TREM2 to dysregulate neuroinflammation. *J Neuroinflammation*. 2020;17(1):351.
41. Casali BT, Landreth GE. Aβ extraction from murine brain homogenates. *Bio Protoc*. 2016;6(8):e1787.
42. Zhang X, Goncalves R, Mosser DM. The isolation and characterization of murine macrophages. *Curr Protoc Immunol*. 2008;83(1): 14.11.11–14.11.14.
43. Prokop S, Miller KR, Labra SR, *et al*. Impact of TREM2 risk variants on brain region-specific immune activation and plaque microenvironment in Alzheimer's disease patient brain samples. *Acta Neuropathol*. 2019;138(4):613–630.
44. Gu Z, Eils R, Schlesner M. Complex heatmaps reveal patterns and correlations in multidimensional genomic data. *Bioinformatics*. 2016;32(18):2847–2849.
45. Gratuze M, Leyns CEG, Holtzman DM. New insights into the role of TREM2 in Alzheimer's disease. *Mol Neurodegener*. 2018;13(1): 66.
46. Wang Y, Cella M, Mallinson K, *et al*. TREM2 lipid sensing sustains the microglial response in an Alzheimer's disease model. *Cell*. 2015;160(6):1061–1071.
47. Heneka MT, Kummer MP, Stutz A, *et al*. NLRP3 is activated in Alzheimer's disease and contributes to pathology in APP/PS1 mice. *Nature*. 2013;493(7434):674–678.
48. Ising C, Venegas C, Zhang S, *et al*. NLRP3 inflammasome activation drives tau pathology. *Nature*. 2019;575(7784):669–673.
49. Gowrishankar S, Yuan P, Wu Y, *et al*. Massive accumulation of luminal protease-deficient axonal lysosomes at Alzheimer's disease amyloid plaques. *Proc Natl Acad Sci USA*. 2015;112(28): E3699–E3708.
50. Preische O, Schultz SA, Apel A, *et al*. Serum neurofilament dynamics predicts neurodegeneration and clinical progression in presymptomatic Alzheimer's disease. *Nat Med*. 2019;25(2): 277–283.
51. Francistiová L, Bianchi C, Di Lauro C, *et al*. The role of P2X7 receptor in Alzheimer's disease. *Front Mol Neurosci*. 2020;13:94.
52. Wang H, Bloom O, Zhang M, *et al*. HMG-1 as a late mediator of endotoxin lethality in mice. *Science*. 1999;285(5425):248.
53. Chen H, Kwong JC, Copes R, *et al*. Living near major roads and the incidence of dementia, Parkinson's disease, and multiple sclerosis: A population-based cohort study. *Lancet*. 2017;389-(10070):718–726.
54. Oudin A, Forsberg B, Adolfsson AN, *et al*. Traffic-related air pollution and dementia incidence in Northern Sweden: A longitudinal study. *Environ Health Perspect*. 2016;124(3):306–312.
55. Power MC. Growing evidence links air pollution exposure to risk of Alzheimer's disease and related dementia. *Brain*. 2020;143(1): 8–10.
56. Jew K, Herr D, Wong C, *et al*. Selective memory and behavioral alterations after ambient ultrafine particulate matter exposure in aged 3xTgAD Alzheimer's disease mice. *Part Fibre Toxicol*. 2019;16(1):45.
57. Sobolewski M, Abston K, Conrad K, *et al*. Lineage- and sex-dependent behavioral and biochemical transgenerational consequences of developmental exposure to lead, prenatal stress, and combined lead and prenatal stress in mice. *Environ Health Perspect*. 2020;128(2):027001.
58. Erickson MA, Jude J, Zhao H, *et al*. Serum amyloid A: an ozone-induced circulating factor with potentially important functions in the lung-brain axis. *FASEB J*. 2017;31(9):3950–3965.
59. Tyler CR, Noor S, Young TL, *et al*. Aging exacerbates neuroinflammatory outcomes induced by acute ozone exposure. *Toxicol Sci*. 2018;163(1):123–139.
60. Zera KA, Buckwalter MS. The local and peripheral immune responses to stroke: implications for therapeutic development. *Neurotherapeutics*. 2020;17(2):414–435.
61. Bratton SL, Davis RL. Acute lung injury in isolated traumatic brain injury. *Neurosurgery*. 1997;40(4):707–712.
62. Ritchie K, Chan D, Watermeyer T. The cognitive consequences of the COVID-19 epidemic: collateral damage? *Brain Commun*. 2020;2(2).
63. Hampshire A, Trender W, Chamberlain SR, *et al*. Cognitive deficits in people who have recovered from COVID-19. *EClinicalMedicine*. 2021;39:101044.
64. Helms J, Kremer S, Merdji H, *et al*. Neurologic features in severe SARS-CoV-2 infection. *N Engl J Med*. 2020;382(23):2268–2270.